ELSEVIER

Dynamics of Atmospheres and Oceans 24 (1996) 27–39

dynamics of atmospheres and oceans

Comparison of diapycnal diffusivity measured by tracer and microstructure techniques

A. Wüest [a,*], D.C. van Senden [a], J. Imberger [b], G. Piepke [a], M. Gloor [a]

[a] *Swiss Federal Institute for Environmental Science and Technology (EAWAG) and Swiss Federal Institute of Technology (ETH), CH-8600 Dübendorf, Switzerland*

[b] *Centre for Water Research, University of Western Australia, Nedlands, Perth, W.A. 6009, Australia*

Received 10 October 1994; revised 3 April 1995; accepted 5 April 1995

Abstract

Estimates of vertical diffusivity inferred from microstructure measurements in the thermocline of the open ocean (approximately 0.1 $cm^2\ s^{-1}$) are typically an order of magnitude smaller than values obtained with basin-wide tracer balances (approximately 1 $cm^2\ s^{-1}$). To evaluate this seeming discrepancy between these two methods, a comparison study was conducted in the hypolimnion of Lake Alpnach (Switzerland) over a period of 1 month. Diapycnal tracer diffusivity was estimated from the vertical spreading of SF_6 and from the heat budget, whereas the microstructure-based diapycnal diffusivity was calculated from the dissipation of turbulent kinetic energy measured with a high-resolution temperature profiler.

The microstructure measurements revealed that the boundary layer above the sediment is the most turbulent zone in the hypolimnion. Based on two assumptions for the functional form of the buoyancy flux in the bottom boundary layer, horizontally averaged microstructure diffusivities and basin-wide tracer diffusivities agree to within a factor of two. We conclude that (1) the apparent paradox is not due to insufficiencies in the microstructure method and (2) the two techniques yield the same diapycnal diffusivity if the effects of boundary mixing are included in the basin-wide comparison. This conclusion implies that basin-wide diapycnal diffusivity in the ocean thermocline is indeed an order of magnitude larger than mixing in the ocean interior. This is consistent with the results of recent tracer and microstructure measurements conducted in the thermocline of the open ocean.

* Corresponding author.

0377-0265/96/$15.00 © 1996 Elsevier Science B.V. All rights reserved
SSDI 0377-0265(95)00408-4

1. Introduction

Vertical profiles of heat, salt, density and geochemical compounds in the thermocline of the ocean depend on their turbulent fluxes across isopycnal surfaces. The vertical structure of the thermocline can be considered to result from the balance of the thermohaline circulation, transporting cold, heavy water downward to the abyssal ocean, and the upward turbulent diapycnal flux of density. The question of the intensity of turbulent diapycnal mixing in the ocean thermocline and the mechanisms driving it is therefore of fundamental geophysical importance.

Estimates of vertical diffusivity in the ocean thermocline differ by about a factor of ten. Indirect estimates come from fitting one-dimensional models to vertical tracer profiles and assuming a balance between upward advection and turbulent downward diffusion. These models yield a tracer-based diffusivity K_t close to the canonical value of 1 $cm^2\ s^{-1}$ (Munk, 1966; Gargett, 1984; Li et al., 1984). Direct estimates of diapycnal diffusivity K_ϵ stem from measurements of the dissipation of turbulent kinetic energy ϵ, which is based on the microstructure technique (Osborn, 1980). Assuming a balance between the turbulent production of potential energy ($K_\epsilon N^2$) and dissipation ϵ yields $K_\epsilon = \gamma_{mix}\epsilon N^{-2}$ (where γ_{mix} is mixing efficiency, $N^2 = -g\rho^{-1}(\partial\rho/\partial z)$ is stability, g is acceleration due to gravity, ρ is density and z is vertical coordinate, positive upwards). Even for background internal wave levels (Gregg and Sanford, 1988), the microstructure-based estimates K_ϵ are typically an order of magnitude less (Gregg, 1987) than the values of K_t inferred indirectly from tracers.

This study attempts to explain this seeming paradox between the two methods. The discrepancy between the estimated diffusivities K_t and K_ϵ can be explained by two hypotheses: (1) the indirect tracer method, which involves averaging over different mixing processes, including those occurring in the boundary regions, yields larger values than those derived from open-ocean microstructure profiles, which are sensitive only to processes in the interior of the water body; or (2) the dissipation method is biased owing to uncertainty about the mixing efficiency γ_{mix}, sampling sufficiency or other method-related assumptions (Osborn, 1980) and is yielding values which are too small. The comparison study described here was carried out in the hypolimnion of a lake over the period of 1 month to test the second hypothesis. We determined the diapycnal tracer diffusivities K_t from the vertical spreading of deliberately injected sulphur hexafluoride (SF_6) and from the heat budget (Powell and Jassby, 1974) and compared it with diapycnal dissipation diffusivities K_ϵ inferred from temperature microstructure data taken during the 1 month measuring campaign. A density-stratified lake was chosen for this study, because (1) diapycnal mixing in the hypolimnion is caused by small-scale turbulence, as it is in the open ocean, (2) hypolimnetic diapycnal tracer diffusivities (Imberger and Patterson, 1989; Heinz et al., 1990; Imboden and Wüest, 1995) are similar to oceanic thermocline dissipation diffusivities, and (3) the tracer balance is relatively well defined in an enclosed hypolimnion.

The experimental set-up, measurement techniques and data analysis are explained in Section 2. The physical background conditions of the lake and the

diffusivities determined are presented in Section 3. After comparing the diffusivities in Section 4, conclusions related to the discrepancy of the two methods are drawn.

2. Experiment

The comparison study was conducted in July 1989 in Lake Alpnach (Fig. 1), where local wind exposure leads to basin-wide diapycnal tracer diffusivities comparable with values found in the thermocline of the open ocean. Lake Alpnach has a length of about 5 km, a width of about 1 km, and a maximum depth of 34 m (Fig. 1). In July, density stratification is strong and almost unaffected by dissolved solids (salinity about 0.3‰). Fig. 2 shows temperature and stability averaged from 82 CTD (conductivity–temperature–depth) profiles taken during the study. Wind forcing was measured near the centre of the lake at a buoy-mounted automatic meteorological station and the excited internal motions along the lake axis were

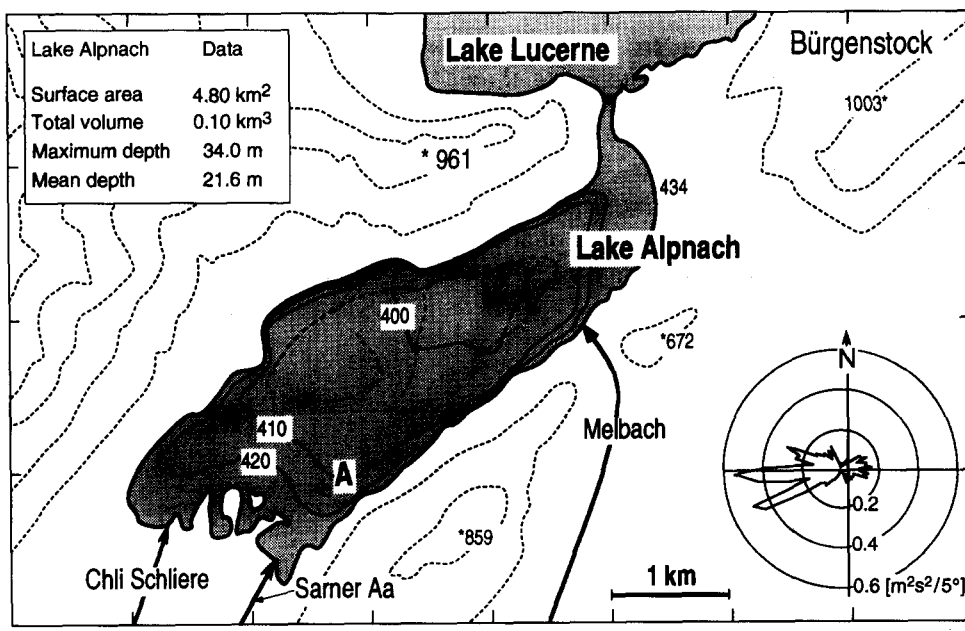

Fig. 1. Map of Lake Alpnach (central Switzerland). +, Locations of thermistor strings, labelled A (length 20 m), M (30 m) and N (15 m). A meteorological buoy was moored at M. Depth contours, lake surface elevation and heights of nearby mountains (asterisks) are given in metres above sea-level. The outlet of Lake Alpnach is a passage 3 m deep connecting Lake Alpnach to Lake Lucerne. SF_6 tracer was released in two streaks (over about 6 km) represented by the dashed line. Inset: cumulative distribution of the square of the wind speed at Mooring M (vectors shown in the direction of the wind). Adapted from Münnich et al. (1992).

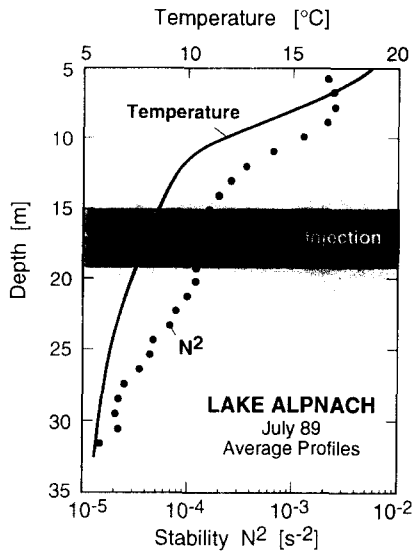

Fig. 2. Temperature and stability N^2 averaged from 82 CTD profiles taken during the 1 month study. Sampling dates are labelled T in Fig. 3. The dark and light shading represent the initial and final standard deviations, respectively, of the SF_6 concentration.

monitored at 10 min intervals using three Aanderaa thermistor strings (Fig. 1), each consisting of 11 evenly spaced sensors.

SF_6 was chosen as a tracer as it is an inert and non-toxic compound of low background concentration which has proven to be conservative in subsurface water (Watson et al., 1987). During a period of 3.5 h, approximately 54 g of SF_6 were released in two streaks at a depth of about 17 m over a total length of about 6 km (Fig. 1; Table 1). SF_6 was dissolved in water in a crossflow tube on the ship deck

Table 1
Tracer injection data

Lake	
Target injection temperature (T)	8.0°C
Mean depth at $T = 8$°C	17.0 m
Vertical temperature gradient at injection depth ($\partial T/\partial z$)	0.25°C m^{-1}
Stability at injection depth (N^2)	1.3×10^{-4} s^{-2}
Isobath area at injection depth (A)	3.2 km^2
Sediment surface area per unit volume of water at injection depth ($\partial A/\partial V$)	0.023 m^{-1}
Tracer	
Amount of SF_6 injected	54 ($\pm$ 5%) g (= 17 g km^{-2})
Total length of SF_6 streaks	$\approx$ 6 km
Solubility of SF_6 at $T = 8$°C	65 g m^{-3} atm^{-1}
SF_6 concentration in injected water	9–15 g m^{-3}
Water pump rate	10–20 l min^{-1}

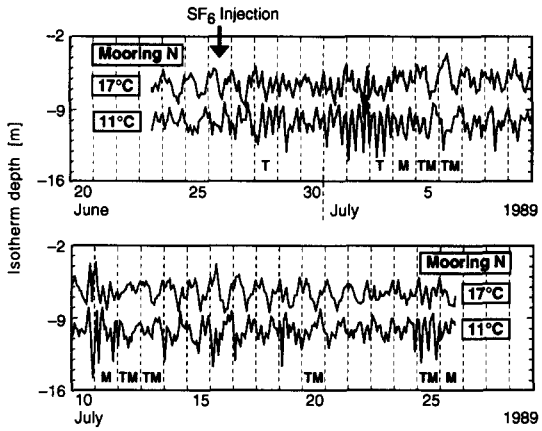

Fig. 3. Time series of the depths of two selected isotherms calculated from thermistor chain data taken at Mooring N (Fig. 1). The data were low-pass filtered with a cutoff at 2.5 h. Two main periodicities (7.5 h and 24 h) are obvious. The shorter period (see e.g. 11 July) represents the first vertical mode, and the 24 h seiching (e.g. 14–20 July) the second mode (Münnich et al., 1992). Dates of SF_6 and CTD casts (T), microstructure profiles (M) and SF_6 release are indicated.

(Schlatter, 1991), pumped to the target depth and released through eight nozzles, each of 3.5 mm diameter. To minimize the initial diapycnal spread of SF_6, injection was adjusted to the isopycnal surface corresponding to the 8°C isotherm (Fig. 2) using a small CTD probe. The 8°C isotherm has been chosen as an ideal compromise of different constraints. The water temperature was recorded close to the nozzles, allowing the vertical displacement from the target isotherm during injection to be determined. The calculated initial vertical variance of the tracer distribution of $\sigma_0^2 \approx 4.4$ m^2 (see Fig. 4 below) fits well to the in situ tracer distributions found during the following few days.

To determine the diapycnal spreading during the 1 month study, 57 SF_6 profiles were collected on eight separate days (Fig. 3) using an array of Niskin bottles. SF_6 was stripped from a 25 ml subsample into a 25 ml headspace containing nitrogen. Subsequently, the SF_6 was measured using a gas chromatograph with an electron-capture detector (Schlatter et al., 1990). To achieve statistically representative vertical variances of the tracer distribution, we averaged the profiles to obtain daily means. Simultaneously measured CTD profiles allowed the SF_6 sample depth to be matched with temperature (density), to remove reversible displacements owing to internal seiching: SF_6 profiles were averaged in bins of constant temperature and averages were retransferred to depth using the daily mean temperature profiles. Finally, the diapycnal tracer diffusivity K_t of SF_6 was determined by calculating the temporal rate of spread of the vertical tracer variance $\sigma^2(t)$ and using the relation $K_t = 0.5 \mathrm{d}\sigma^2(t)/\mathrm{d}t$ (Fig. 4). We consider this tracer diffusivity to include the effects of boundary mixing arising above the sediment surface, which bounds the lake near 17 m depth (Table 1).

The diapycnal tracer diffusivity K_t was determined independently by using the heat budget method (Powell and Jassby, 1974; Heinz et al., 1990). It is based on

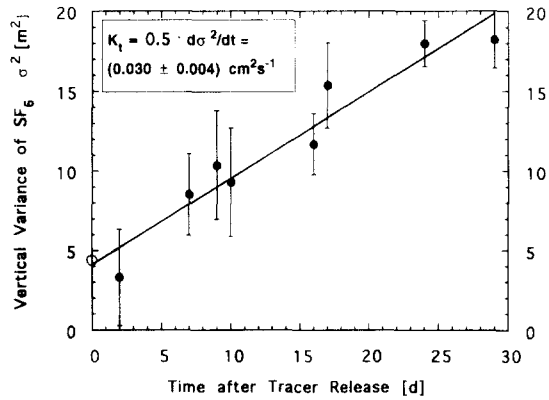

Fig. 4. Vertical variance σ^2 of the concentration of the tracer SF_6 as a function of time after tracer release (26 June; Fig. 3). $K_t = 0.5 d\sigma^2/dt$ was determined by linear regression. The fitted initial variance σ_0^2 is close to the value determined by continuous CTD recording during tracer release (open circle on vertical axis). The errors of the variances were determined by fitting a Gaussian distribution to the vertical profiles.

the assumption that at depth z, the vertical turbulent transport of heat is equal to the rate of change of heat content below z, given by

$$\rho c_p K_t(z) A(z) \frac{\partial T(z)}{\partial z} \int_{max.\ depth}^{z} \rho c_p A(z') \frac{\partial T(z')}{\partial t} dz'$$

where $A(z)$ is the cross-sectional lake area at z and c_p is the specific heat. Temperature changes $\partial T(z')/\partial t$ were determined based on data from two Aanderaa thermistor strings (the mid-lake string M (Fig. 1) failed after 10 days) and 82 CTD profiles, which also allowed the average vertical temperature gradients

Table 2
Comparison of diapycnal diffusivities at 17 m depth

Method	Formula applied	K ($cm^2\ s^{-1}$)
Basin-wide tracer diffusivity		
SF_6	$K_t = (1/2)(\partial\sigma^2/\partial t)$	0.030 ± 0.004
Temperature	$K_t = \int_{max.depth}^{z} A(z')(\partial T(z', t)/\partial t) dz' [A(z)(\partial T(z)/\partial z)]^{-1}$	0.037 ± 0.004
Horizontally averaged dissipation diffusivity		
(a) Integration to δ_ν [a]	$K_\epsilon = (\gamma_{mix}/N^2)[\epsilon_I + (\partial A/\partial V)(u^3_*/k)\ln(\delta_B/\delta_\nu)]$	0.032 ± 0.011
(b) Constant buoyancy flux [b]	$K_\epsilon = (\gamma_{mix}/N^2)[\epsilon_I + (\partial A/\partial V)(u^3_*/k)[1 + \ln(\delta_B/\delta_{mix})]]$	0.018 ± 0.007

[a] Integration down to the viscous layer of thickness $\delta_\nu = 10\nu/u_* = 0.8$ cm; ϵ_I is the dissipation in the interior (Fig. 5(a); N^2 is the stability (Fig. 2); $u_* = 0.19$ cm s^{-1} is the friction velocity; $k = 0.41$ is von Kàrmàn's contant; $\delta_B = 10$ m is the thickness of the Prandtl layer; $\gamma_{mix} = 0.12$ (Peters and Gregg, 1988); $\partial A/\partial V$ is the sediment surface area per unit volume of water (Table 1); ν is the kinematic viscosity.
[b] Assumption of constant buoyancy flux in the homogenized bottom layer of thickness $\delta_{mix} = 0.5$ m, which was determined from the CTD profiles reaching the lake bottom near 17 m depth.

$\partial T(z)/\partial z$ to be calculated precisely. Finally, the temperature-based diapycnal tracer diffusivity K_t was determined using the formula given in Table 2.

On nine different days (Fig. 4), 130 temperature microstructure profiles were measured using a self-contained profiler (Carter and Imberger, 1986), rising at about 0.1 m s^{-1} and collecting data at 100 Hz from a pair of fast-response thermistors (FP-07). Data were filtered as required for response matching (Fozdar et al., 1985). To detect the turbulent mixing sections, an algorithm based on a stationary turbulence criterion was employed (Imberger and Ivey, 1991). This algorithm allowed the vertical temperature microstructure profiles to be divided into turbulent and non-turbulent segments. Power spectra were calculated for both types of segment, allowing the dissipation of turbulent kinetic energy ϵ to be determined by fitting the measured spectra to Batchelor's model spectrum (Gibson and Schwartz, 1963; Dillon and Caldwell, 1980). The quality of each individual fit was checked by eye, and subsequent analyses were carried out using only the data from those turbulent segments which followed the characteristic Batchelor spectrum. The non-turbulent segments do not bias the averaged dissipation rate, as the spectra of those segments definitely did not follow Batchelor's form and their spectral content indicated dissipation to be low. The error introduced owing to ambiguous spectra is far below the statistical uncertainty of the dissipation estimate.

For each of the 130 profiles, bin-averaged dissipation estimates were obtained for 'depth bins' beginning at the lake surface and extending downwards (Fig. 5(a)). As it became obvious that turbulence was higher near the bottom boundary, we also calculated the arithmetic means for 'height bins' beginning 0.5 m above the lake bottom and extending upwards (Fig. 5(b)). Averages of dissipation were weighted with the segment length by assuming zero dissipation outside the turbulent segments. As most of the observed hypolimnion is non-turbulent, the averages are clearly lower than the dissipation within individual turbulent segments. The

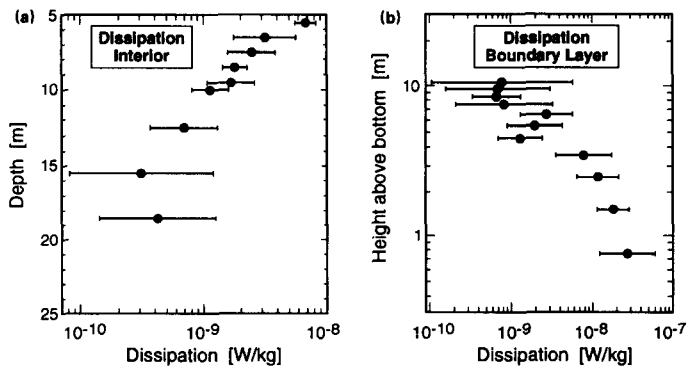

Fig. 5. Average dissipation determined from 130 profiles: (a) averaged in 'depth bins'; (b) averaged in 'height bins' (parallel to the lake bottom). Error bars represent the standard deviations of $\ln(\epsilon)$ of the maximum likelihood estimate.

arithmetic mean and the maximum likelihood estimate (Baker and Gibson, 1987) were both calculated.

3. Observations

3.1. Wind and internal seiches

Atmospheric convection along the nearby mountains stimulated a predominantly diel wind blowing regularly and uniformly parallel to the major axis (Fig. 1; for details see Münnich et al. (1992)). The excited internal seiching motion, responsible for hypolimnetic diapycnal mixing, is shown in Fig. 3. Spectral analysis revealed two dominant periodicities that correspond to the first vertical first horizontal and second vertical first horizontal seiche modes (Münnich et al., 1992). A subsequent field campaign showed that for both modes, bottom currents along the major axis of the lake correlate perfectly with the displacements of the hypolimnetic isotherms in Fig. 3 (Gloor et al., 1994). The corresponding phases reveal that the whole hypolimnetic water body is excited by first horizontal seiche modes. With this simple structure it was possible to estimate the basin-wide hypolimnetic velocity field by a topography-dependent seiche model (Münnich, 1993). Thus we were able to identify the regions of high seiche-induced vertical shear relevant to diapycnal mixing; i.e. the interior of the upper thermocline and the boundary layer above the sediment. This knowledge of the vertical structure of the currents permitted the computation of horizontal averages of the diapycnal dissipation diffusivity.

3.2. Vertical spreading of SF_6

As SF_6 was released over about 6 km (Fig. 1) the tracer was distributed rapidly all over the 8°C isopycnal surface area of 3.2 km^2 (Table 1) and subsequently SF_6 was found in all profiles, even 2 days after injection. Isopycnal diffusion coefficients (quantifying the rate of spread along isopycnal surfaces) which have been determined in various Swiss lakes including Lake Alpnach (Peeters, 1994), are about 0.5 $m^2\ s^{-1}$ for that length scale. Therefore the SF_6 in 17 m depth can be expected to reach the sediment boundary, typically at about 0.5 km from the injection line (Fig. 1), in about 5 days. Indeed, within the first 10 days after injection, SF_6 concentrations found in individual profiles were very variable: on Day 7, for instance, SF_6 content varied by a factor of three among the profiles.

In Fig. 4 the vertical variances σ^2 of the SF_6 distributions are shown as a function of time after tracer injection. The daily averaged SF_6 profiles were constructed, as explained in Section 2, by removing reversible displacements owing to seiches. Within the 1 month period, σ increased from 2.1 m to 4.3 m. Linear regression in Fig. 4 gives a diapycnal tracer diffusivity of $K_t = 0.5\partial\sigma^2/\partial t = 0.030 \pm 0.004\ cm^2\ s^{-1}$. The fit yields an initial variance σ_0^2 of 4 m^2 (Fig. 4), which agrees very well with the initial variance of 4.4 m^2 estimated from the CTD record during

SF_6 injection. This agreement supports the view that the tracer quickly reached the sediment boundary and that the SF_6 profiles consequently allow a basin-wide diapycnal diffusivity to be computed. From the SF_6 data, however, it is not possible to determine exactly when the tracer hit the sediment, as the tracer variance is not well enough resolved during the first few days after injection. Based on the time scale given above, we expect that the value of K_t slightly underestimates (about 10%) the representative basin-wide diapycnal tracer diffusivity.

3.3. Heat budget

The result of the heat budget method agrees with this conclusion. The diapycnal diffusivity was calculated in the vicinity of 17 m depth using temperature as a tracer and applying the equation in Table 2. As SF_6 is approximately normally distributed relative to 17 m depth, temperature-based diffusivity was also weight-averaged by a Gaussian curve with the representative standard deviation of $\sigma = 3.2$ m. The result $K_t = 0.037 \pm 0.004$ cm^2 s^{-1} not biased by this procedure, as K_t is vertically constant within the margin of error close to 17 m depth. We consider this value also to represent a basin-wide diapycnal diffusivity, including the effect of mixing in the boundary layer above the sediment.

3.4. Dissipation

Arithmetic means of dissipation $\bar{\epsilon}$, averaged in vertical 'depth bins' (over the 130 profiles), cannot be used directly to calculate diapycnal diffusivity as these horizontal averages do not necessarily yield a representative dissipation. Because many profiles extended to depths greater than 17 m, the upper thermocline averages contain data mainly from the interior of the hypolimnion, whereas deep-water averages are dominated by turbulence above the sediment boundary. To obtain adequate averages, we have divided the water column into two regions: 'interior' (distance from sediment greater than 10 m) and 'boundary layer'. A distance of 10 m was considered reasonable to distinguish between 'boundary' and 'interior', as the dissipation 10 m above the sediment falls to background level.

Fig. 5 displays separate arithmetic averages for the two regions in 'depth bins' (Fig. 5(a)) and in 'height bins' (above the sediment: Fig. 5(b)). Dissipation in the interior region decreases with depth, rapidly reaching the limit of detection (Fig. 5(a)), whereas dissipation increases towards the sediment (Fig. 5(b)). This increase is approximately proportional to h^{-1} (h is the distance to the local sediment bottom), as predicted by classical boundary-layer theory. Fitting the scaling relation $\epsilon = u^3_*(kh)^{-1}$ to the data in Fig. 5(b) yields a friction velocity of $u_* = 0.19$ cms^{-1} which corresponds to a typical velocity of $(C_{1\,\mathrm{m}})^{-1/2}u_* = 5$ cms^{-1} at 1 m above the bottom ($C_{1\,\mathrm{m}} = 1.6 \times 10^{-3}$ is the drag coefficient (Elliott, 1984), and $k = 0.41$ is von Kàrmàn's constant). This value is representative of Lake Alpnach for the time of year (Gloor, 1995). The arithmetic mean, as well as the maximum likelihood estimate (Baker and Gibson, 1987) of the dissipation profile ϵ were in agreement within the standard deviation of $\ln(\epsilon)$, plotted as error bars in Fig. 5.

4. Comparison and conclusion

4.1. Comparison

Like dissipation, the average buoyancy flux (the rate of production of potential energy, $K_\epsilon N^2$) between 14 and 20 m depth, where most of the SF_6 was located, is comprised of contributions from the 'interior' of the water body and from the 'boundary layer'. Two different models (Table 2) were applied to form horizontal averages. For case (a) we use the scaling relation $\epsilon = u_*^3 (kh)^{-1}$ fitted to the data (in Fig. 5(b)) to extrapolate the dissipation from 0.5 m down to the upper boundary of the viscous layer (of thickness δ_ν). Further, we assume that the buoyancy flux is a constant fraction γ_{mix} of dissipation throughout the boundary layer. For case (b) we assume that there is a homogenized layer of thickness δ_{mix} above the sediment, which forms as a result of the intense mixing occurring there. Consequently, for case (b), the buoyancy flux increases towards the sediment, as in (a), but remains constant within the homogenized bottom layer.

The results of the two methods used to compute horizontal averages are given in Table 2, where the integration formula and all parameter values are also summarized. Case (a) evidently yields a larger value, as (a) contains the assumption that the water column is stratified all the way to the sediment. Therefore (a) probably yields an overestimate of the buoyancy flux and consequently also of the diapycnal diffusivity $K_\epsilon = 0.032 \pm 0.011$ cm^2 s^{-1} (Table 2). Model (b) is based on a more realistic assumption, as mixing in a homogenized layer (of thickness δ_{mix}) is less efficient. The value of diapycnal diffusivity $K_\epsilon = 0.018 \pm 0.007$ cm^2 s^{-1} (Table 2) is, however, most probably an underestimate, as 'homogenized' layers hardly ever had neutral stability (Gloor et al., 1994). We assume the 'truth' to lie somewhere between, and set $K_\epsilon = 0.025$ cm^2 s^{-1} for the following comparison.

The tracer diffusivities of SF_6 (0.030 cm^2 s^{-1}) and temperature (0.037 cm^2 s^{-1}) agree within the relevant margin of error (Table 2). For the comparison, we also set the average K_t to 0.033 cm^2 s^{-1}, as SF_6 provides a potential underestimate (see above) and temperature a potential overestimate (owing to the existence of heat sources not included in the heat budget calculation). Consequently, tracer and microstructure diffusivity values agree to within a factor of 1.3. Several sources of uncertainty may contribute to this factor:

(1) for the mixing efficiency, we used the value $\gamma_{mix} = 0.12$ (Peters and Gregg, 1988), which is, however, not well established. Agreement between K_t and K_ϵ could be achieved using $\gamma_{mix} = 0.16$, a value still below but comparable with the well-known value $\gamma_{mix} = 0.2$ (Osborn, 1980) used in oceanic microstructure work (Gregg and Sanford, 1988; Toole et al., 1994).

(2) Even though the diel wind and internal seiching were fairly uniform, we can expect dissipation in the hypolimnion to be intermittent. To estimate the degree of undersampling, we calculated the wind energy input (proportional to the cube of the wind speed) by first averaging the wind speed over 6 h, equivalent to a quarter of the prominent seiching period (Spigel and Imberger, 1980). Comparing the wind energy input during microstructure sampling (including the previous 12 h) with the

entire period of 1 month revealed that the energy input during sampling was lower than average by a factor of 1.4. This suggests that the microstructure diffusivity was indeed underestimated by a factor comparable to 1.3, the factor of disagreement between K_t and K_ϵ.

(3) Even though the basin shape is simple, resolution of the bottom velocity distribution by the topography-dependent seiche model of Münnich (1993) is unlikely to be perfect; it is therefore unrealistic to expect an agreement better than a factor of 1.3.

4.2. Conclusions

Despite the fact that the diapycnal diffusivity estimates K_t and K_ϵ, based on tracer and microstructure data, respectively, disagree by a factor of 1.3, we can clearly draw the following conclusions:

(1) within the vertical range of interest, i.e. between 14 and 20 m depth, dissipation in Lake Alpnach is dominated by turbulence within the bottom boundary layer.

(2) Diapycnal diffusivity is due to a combination of buoyancy flux originating in the interior of the water body and within the bottom boundary layer. If both sources are adequately taken into account, the diapycnal diffusivity determined from tracer and microstructure data agree to within less than a factor of two.

(3) Consequently, the microstructure diffusivity estimates from the thermocline of the open ocean, which are of the order of 0.1 $cm^2\ s^{-1}$, are not a factor of ten too low, but in fact are correct. This implies that mixing in the thermocline of the open ocean is indeed an order of magnitude less than the basin-wide diapycnal diffusivity of 1 $cm^2\ s^{-1}$. Recent tracer measurements in the thermocline of the open ocean (Ledwell et al., 1993) and microstructure estimates in the interior as well as at the sediment boundary of the ocean thermocline (Toole et al., 1994) support this conclusion. Taken together, these results suggest that basin-wide diffusivity may be dominated by bottom boundary processes both in lakes and in the ocean. Consequently, the effects of mixing in the bottom boundary layer have to be included in future studies on diapycnal diffusivity in all stratified natural waters.

Acknowledgements

We are in debt to many people from the Environmental Physics Department at EAWAG for their generous support in the field: M. Hofer, D.M. Imboden, M. Münnich, F. Peeters, J. Schlatter, M. Ulrich, and especially to M. Schurter for his unfailing presence on the lake. We are also grateful to V. Graf, H. Bolliger and D.M. Livingstone for typing, drawing and improving the English, respectively. Further, we acknowledge the constructive criticism of an anonymous reviewer. This work was supported by Swiss National Science Foundation Grants 20-27751.89 and 20-32700.91.

References

Baker, M.A. and Gibson, C.H., 1987. Sampling turbulence in the stratified ocean: statistical consequences of strong intermittency. J. Phys. Oceanogr., 17: 1817–1836.

Carter, G.D. and Imberger, J., 1986. Vertically rising microstructure profiler. J. Atmos. Oceanic Technol., 3: 462–471.

Dillon, T.M. and Caldwell, D.R., 1980. The Batchelor spectrum and dissipation in the upper ocean. J. Geophys. Res., 85: 1910–1916.

Elliott, J.A., 1984. Measurement of the turbulence in an abyssal boundary layer. J. Phys. Oceanogr., 14: 1778–1786.

Fozdar, F.M., Parker, G.J. and Imberger, J., 1985. Matching temperature and conductivity sensor response characteristics. J. Phys. Oceanogr., 15: 1557–1569.

Gargett, A.E., 1984. Vertical eddy diffusivity in the ocean interior. J. Mar. Res., 42: 359–393.

Gibson, C.H. and Schwartz, W.H., 1963. The universal equilibrium spectra of turbulent velocity and scalar fields. J. Fluid Mech., 16: 365–384.

Gloor, M., 1995. Studium der Randmischung in geschichteten Wasserkörpern mit Hilfe der Temperaturmikrostrukturmethode. Ph.D. Diss., ETH, Zürich, in preparation.

Gloor, M., Wüest, A. and Münnich, M., 1994. Benthic boundary mixing and resuspension induced by internal seiches. Hydrobiologia, 284: 59–68.

Gregg, M.C., 1987. Diapycnal mixing in the thermocline: a review. J. Geophys. Res., 92: 5249–5286.

Gregg, M.C. and Sanford, T.B., 1988. The dependence of turbulent dissipation on stratification in a diffusively stable thermocline. J. Geophys. Res., 93: 12381–12392.

Heinz, G., Ilmberger, J. and Schimmele, M., 1990. Vertical mixing in Überlingersee, western part of Lake Constance. Aquat. Sci., 52: 256–268.

Imberger, J. and Patterson, J.C., 1989. Physical Limnology. Advances in Applied Mechanics. Academic Press, Cambridge, pp. 303–475.

Imberger, J. and Ivey, G.N., 1991. On the nature of turbulence in a stratified fluid, part II: Application to lakes. J. Phys. Oceanogr., 21: 659–679.

Imboden, D.M. and Wüest, A., 1995. Mixing mechanisms in lakes. In: A. Lerman, D.M. Imboden and J.R. Gat (Editors), Physics and Chemistry of Lakes. Springer, Heidelberg, pp. 83–138.

Ledwell, J.R., Watson, A.J. and Law, C.S., 1993. Evidence for slow mixing across the pycnocline from an open-ocean tracer-release experiment. Nature, 364: 701–703.

Li, Y.-H., Peng, T.-H., Broecker, W.S. and Oestlund, H.G., 1984. The average vertical mixing coefficient for the oceanic thermocline. Tellus, 36B: 212–217.

Münnich, M., 1993. On the influence of bottom topography on the vertical structure of internal seiches. Ph.D. Dissertation, ETH, Zürich, 97 pp.

Münnich, M., Wüest, A. and Imboden, D.M., 1992. Observations of the second vertical mode of the internal seiche in an alpine lake. Limnol. Oceanogr., 37: 1705–1719.

Munk, W.H., 1966. Abyssal recipes. Deep-Sea Res., 13: 707–730.

Osborn, T.R., 1980. Estimates of the local rate of vertical diffusion from dissipation measurements. J. Phys. Oceanogr., 10: 83–89.

Peeters, F., 1994. Horizontale Mischung in Seen. Ph.D. Dissertation, ETH, Zurich, 147 pp.

Peters, H. and Gregg, M.C., 1988. Some dynamical and statistical properties of equatorial turbulence. In: J.C.J. Nihoul and B.M. Jamart (Editors), Small-scale Turbulence and Mixing in the Ocean, Proc. 19th Int. Colloquium on Ocean Hydrodynamics. Elsevier, New York, pp. 185–200.

Powell, T. and Jassby, A., 1974. The estimation of vertical eddy diffusivities below the thermocline in lakes. Water Resour. Res., 10: 191–198.

Schlatter, J., 1991. Schwefelhexafluorid als Tracer zum Studium von Mischungsprozessen in Seen. Ph.D. Dissertation, ETH, Zurich, 148 pp.

Schlatter, J., Hofer, M. and Imboden, D.M., 1990. Die Verwendung von Schwefelhexafluorid zum Studium von Transportprozessen in Seen. Gas-Wasser-Abwasser, 70: 36–42.

Spigel, R.H. and Imberger, J., 1980. The classification of mixed-layer dynamics in lakes of small to medium size. J. Phys. Oceanogr., 10: 1104–1121.

Toole, J.M., Polzin, K.L. and Schmitt, R.W., 1994. Estimates of diapycnal mixing in the abyssal ocean. Science, 264: 1120–1123.

Watson, A.J. Liddicoat, M.I. and Ledwell, J.R., 1987. Perfluorodecalin and sulphur hexafluoride as purposeful marine tracers: some deployment and analysis techniques. Deep-Sea Res., 34: 19–31.